Journal of Controlled Release 217 (2015) 327–336

Contents lists available at ScienceDirect

Journal of Controlled Release

journal homepage: www.elsevier.com/locate/jconrel

A general model of coupled drug release and tissue absorption for drug delivery devices

Sean McGinty [a,*], Giuseppe Pontrelli [b]

[a] Department of Mathematics and Statistics, University of Strathclyde, Glasgow, UK
[b] Istituto per le Applicazioni del Calcolo — CNR, Via dei Taurini 19, 00185 Roma, Italy

ARTICLE INFO

Article history:
Received 22 June 2015
Received in revised form 24 August 2015
Accepted 14 September 2015
Available online 21 September 2015

Keywords:
Drug delivery
Dissolution
Diffusion
Binding
Two-phase equations
Coupled partial differential equations

ABSTRACT

In this paper we present a general model of drug release from a drug delivery device and the subsequent transport in biological tissue. The model incorporates drug diffusion, dissolution and solubility in the polymer coating, coupled with diffusion, convection and reaction in the biological tissue. Each layer contains bound and free drug phases so that the resulting model is a coupled two-phase two-layer system of partial differential equations. One of the novelties is the generality of the model in each layer. Within the drug coating, our model includes diffusion as well as three different models of dissolution. We show that the model may also be used in cases where dissolution is rapid or not relevant, and additionally when drug release is not limited by its solubility. Within the biological tissue, the model can account for nonlinear saturable reversible binding, with linear reversible binding and linear irreversible binding being recovered as special cases. The generality of our model will allow the simulation of the release from a wide range of drug delivery devices encompassing many different applications. To demonstrate the efficacy of our model we simulate results for the particular application of drug release from arterial stents.

1. Introduction

Local drug delivery devices (DDD) are now common in clinical practice. Examples include drug-eluting stents [1], therapeutic contact lenses [2], transdermal patches [3], and most recently drug-eluting orthopaedic implants [4] (Fig. 1). By targeting the drug exactly at the site where it is required and in a controlled manner, these devices provide a significant advantage over more traditional forms of drug release. For example, with targeted delivery, potentially higher doses of drug can be administered, with less impact on the rest of the body compared with, say, oral drug delivery. Furthermore, there is less input required from the patient who need not worry about forgetting to take their medication. Perhaps the biggest advantage is that the release rate can be controlled, so that the correct dose can be delivered over an extended period of time. From the manufacturing and clinical point of view it is of interest to give careful consideration to the device design so that therapeutic levels of drug are attained in the biological tissue for the necessary period of time. Toxicity can arise if an excessive amount is delivered, or if the drug is released too quickly. On the other hand, the therapeutic action vanishes when the drug concentration drops below a given threshold. The success of the DDD is therefore dependent on the correct extent of drug elution, the rate of release, partitioning, accumulation and binding within the tissue [5]. In this respect, mathematical modelling provides a useful tool to understand the combined action of these processes, and consequently to help devise optimisation strategies for targeted drug delivery [6].

Despite being the subject of intense theoretical and applied research over the past decades [7,8], it is still often unclear exactly what the mechanism of drug release from the DDD is and, as a consequence, even more difficult to predict the drug release kinetics. Nevertheless, countless models have been proposed. Most commonly, diffusion is cited as the dominant release mechanism [9] although dissolution also features heavily in the literature [10]. Furthermore, for certain types of coatings, swelling, erosion and biodegradation have been considered [11,12]. Related to this difficulty is a lack of understanding of molecule transport in the biological tissue, where the drug is targeted. Typically, diffusion and drug binding occur in the tissue, sometimes made of a multilayered structure [13], whilst in some cases there is convection as a result of a pressure gradient across the tissue. In addition, most models deal with the drug release process alone, whilst others consider only the absorption in the tissue. Far fewer models attempt to fully couple a mechanistic description of drug release with tissue absorption [14–19].

Focussing on DDD where the drug is contained within a durable polymer, in this paper we attempt to revisit and classify, in a unifying way, the most popular models and provide a general framework of coupled drug release and tissue absorption. We describe all the dynamics of the drug through its journey from the polymeric coating

* Corresponding author.
E-mail address: s.mcginty@strath.ac.uk (S. McGinty).

http://dx.doi.org/10.1016/j.jconrel.2015.09.025

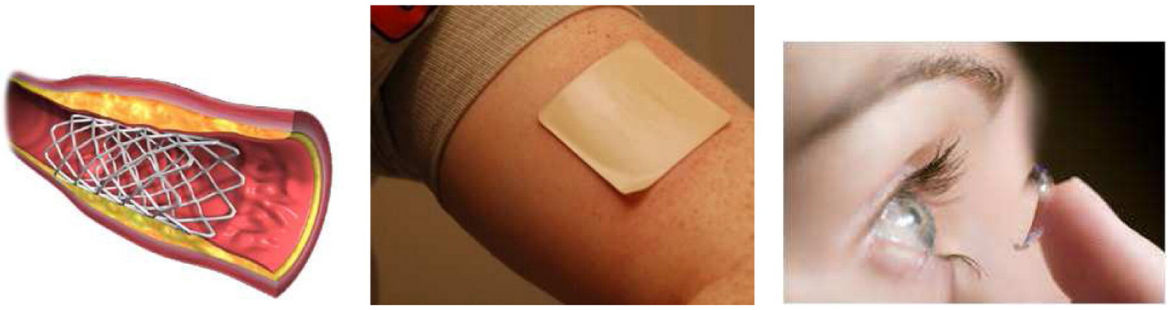

Fig. 1. Examples of DDD. From left to right: coronary stent, transdermal patch, therapeutic contact lens.

where it encapsulated at the manufacture stage, to the cell receptors where it eventually binds. As outlined elsewhere [20], we emphasize here the importance of studying the coupled system, since the drug delivery starts from the polymer and undergoes a cascade of reactions and kinetics as it is first released and then absorbed. Coupled layer systems, together with nonlinear effects, can often produce unexpected results that cannot be predicted by considering each layer alone, nor by superimposing the effects of each layer. This paper is organized as follows. Firstly we provide a description of a general DDD. Then, we focus on the drug coating and present a general model of diffusion–dissolution which includes solubility, before demonstrating a number of special cases. We then proceed to consider the drug transport in biological tissue. We present a general convection–diffusion-reaction model which includes a nonlinear saturable reversible binding model, before outlining how other binding models may be recovered from the general model. We then proceed to describe a suitable numerical method for solving the resulting system of coupled partial differential equations. Due to the contrast of material properties between the two layers, we arrive at a stiff mathematical problem. The method we adopt involves spatial discretization followed by solution of the resulting system of ordinary differential equations. Finally, we present simulated results for one particular example of a DDD, the drug-eluting stent, and we demonstrate that the coupled model is able to predict important characteristics such as the correct duration of the release and the time-varying mass of drug in the tissue.

The benefits of such a comprehensive model, we believe, are twofold. Firstly, it allows designers of DDD to better understand what are the important processes governing the release of drug. Typically this will not be known a priori, but the model provided here, when compared with experimental data, can shed light on this. Secondly, when the important processes have been identified, the model can either be used in its full form (including all of the mechanisms of transport if necessary) or in a simpler form (depending on the particular device and tissue) to predict the effect of varying the design parameters on the release profile and on the drug levels in the biological tissue. Importantly, all of this can be done within the single modelling framework presented here, rather than having to call upon multiple models.

2. The general drug delivery device

In its basic formulation, a DDD consists of a durable structure coated with a thin layer of polymer containing the drug. The structure of the device may be, for example, metallic or polymeric and is often made from a material with markedly different properties to that of the coating. The reason for this is that the polymer coating is designed to control the drug release whilst the device structure generally has another purpose (e.g. to locate the delivery or to act as a scaffold). Whilst the three-dimensional geometry of the device may vary widely (Fig. 1), we can exploit the fact that the coating layer is usually thin relative to its lateral dimensions, with the result being that the drug release predominantly takes place in the direction normal to the device surface [8,21]. This provides justification for an idealized one-dimensional model. The drug coating layer is in contact with biological tissue, where the drug is directed.

As displayed in Fig. 2, let the x-axis be normal to the layer surface and oriented with the positive direction pointing away from the device. Without loss of generality, let $x_0 = 0$ be the interface between the drug coating and the tissue layer, which have thickness l_0 and l_1, respectively, with $l_1 \gg l_0$. The layers are both treated from a macroscopic perspective so that they are represented as two homogeneous porous media. In what follows, the subscripts 0 and 1 indicate parameters and variables with respect to the polymeric matrix and the tissue layer, respectively.

3. Modelling drug release from the polymer matrix

We consider coatings that contain a solid mixture of polymer and drug. Initially the drug is immobile (*encapsulated*) and must dissolve in some release medium before it can be released. When exposed to biofluid, the polymer becomes wetted, initiating a dissolution process, providing a means for the drug to be released from the device. It is often favourable for the drug to be lipophilic, since this can assist with drug retention in the tissue, but at the same time these drugs are typically poorly soluble. Thus the dissolution process is inherently dependent not only on the rate of dissolution (β_0), but also on the solubility of the drug (S) in the release medium. Taking these two factors into account, the overall dissolution process potentially has an important influence on the rate of drug release.

Several different approaches to modelling the dissolution process have been proposed in the literature. These models usually consider the case of initial drug concentration in the coating (B) being higher than the solubility (S) (otherwise the drug is readily dissolved and available for diffusion — see Section 3.1) and can be roughly separated into two distinct classes. In the first approach, a moving boundary problem is considered where drug dissolution occurs on a moving front as fluid penetrates into the polymer coating. Ahead of the moving boundary the immobile drug remains in an encapsulated form but behind the moving front dissolved drug is permitted to leave the coating by diffusion. Dissolution is considered to be instantaneous, with the concentration on the moving front taken to be equal to the drug solubility. This gives rise to a discontinuity of drug concentration: ahead of the moving front the drug is in solid form at concentration equal to its initial value, while behind the moving front the concentration is lower than the solubility [22,23]. In the second approach, which we focus on in this paper, the encapsulated drug is treated as a continuously varying concentration $b_0(x,t)$, and it is assumed that fluid penetrates the porous polymer matrix instantaneously, making it fully wetted [8,14]. The drug dissolution and diffusion through the coating is then described by a

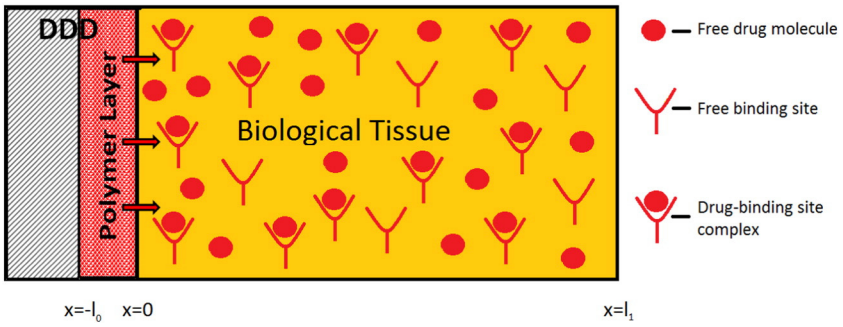

Fig. 2. The geometrical configuration of the DDD. This consists of some durable structure (shaded grey) coated with a thin layer of polymer of thickness l_0 containing the drug (red). The polymer layer is in contact with the biological tissue of thickness l_1 (orange). The drug is transported from the polymer coating via dissolution and diffusion to the tissue where it is subject to diffusion and advection in its free phase and may bind to drug binding sites. Diagram is not to scale. (For interpretation of the references to colour in this figure legend, the reader is referred to the web version of this article.)

system of coupled partial differential equations of the following form:

$$\frac{\partial b_0}{\partial t} = -\beta_0 b_0^{\alpha}(S-c_0) \qquad \text{in}(-l_0,0), \tag{3.1}$$

$$\frac{\partial c_0}{\partial t} = D_0\frac{\partial^2 c_0}{\partial x^2} + \beta_0 b_0^{\alpha}(S-c_0) \qquad \text{in}(-l_0,0), \tag{3.2}$$

where $\alpha = 0,2/3$ or 1, $c_0(x,t)$ is the concentration of dissolved drug, D_0 is the effective diffusion coefficient of the drug through the porous polymer and the dissolution rate β_0 depends upon the porosity of the coating. In the classical Noyes-Whitney approach [24], the rate of dissolution is considered to be proportional to the difference between the drug solubility and the concentration of dissolved drug, yielding a linear equation ($\alpha = 0$). Later modifications by Hixson and Crowell [25] attempted to account for the surface change of dissolving particles, leading to a nonlinear model of dissolution ($\alpha = 2/3$). The value of α is likely to be influenced by the geometrical configuration and chemical properties of drug, as well as the coating manufacture and the device design. Taking this into account, for certain applications, other values of α may in principle be suitable. Therefore, we additionally consider the case of $\alpha = 1$, representing the simplest nonlinear dissolution model that provides a coupling between the free and bound phases.

The case of $\alpha = 2/3$ has been considered in the context of drug-delivery by Frenning [26], and later by Formaggia et al. [14], albeit in a more complicated 2D formulation which includes the effects of polymer degradation. The model (3.1)–(3.2) attempts to unify the dissolution models proposed in the literature, the unit of β_0 $(1/(\mathrm{s}\cdot(\mathrm{mol}\cdot\mathrm{cm}^{-3})^{\alpha}))$ depending on the value of α. It is understood that the above equations hold for the period during which dissolution is ongoing. When all of the solid drug has dissolved (i.e. b_0 reaches zero), the source terms in Eqs. (3.1)–(3.2) are zero. In order to exclude unphysical negative values, one could introduce a Heaviside function as has been done in [8]. However, for clarity of notation we have decided instead to implement this in the numerical algorithm (Section 6).

3.1. Special cases of the diffusion-dissolution model

The model (3.1)–(3.2) accounts for the possibility that the dissolution rate, solubility and rate of diffusion are equally important in determining the rate of release. However, in certain circumstances, one or more of these processes may be insignificant in comparison with the others. For example, DDD which contain drugs with a very high solubility and/or a very low initial drug concentration will readily dissolve and in these cases a pure diffusion model is more appropriate. To estimate the relative magnitude of the competing processes, let us scale time with the typical time-scale for diffusion $t_0' = D_0 t/l_0^2$, and all concentrations with B:

$$b_0' = \frac{b_0}{B}, \quad c_0' = \frac{c_0}{B}, \quad S' = \frac{S}{B}. \tag{3.3}$$

Then Eq. (3.1) becomes:

$$\frac{1}{Da_0^*}\frac{\partial b_0'}{\partial t_0'} = -(b_0')^{\alpha}(S'-c_0'), \tag{3.4}$$

where the nondimensional number $Da_0^* = \beta_0 B^{\alpha} l_0^2/D_0$ (Damköhler number) is the ratio of the diffusion to the dissolution time-scale in the coating (we have used here the superscript * to distinguish this Damköhler number from the corresponding one in Section 5). Immediately we see that in the limit of rapid dissolution (i.e. $Da_0^* \gg 1$) then the left hand side of (3.4) tends to zero and consequently $b_0 \to 0$ and/or $c_0 \to S$. Therefore, on the longer time-scale of diffusion, according to the solubility value, two cases arise:

1) $S' \geqslant 1$: All of the bound drug dissolves instantaneously, so that $b_0 = 0$ and $c_0 = B$. In this case the drug release is diffusion dominated and the purely diffusive mechanism of release can be simulated by selecting values of S and β_0 such that $S \geq B$ and $Da_0^* \gg 1$.
2) $S' < 1$: The free drug phase is saturated instantaneously ($c_0 = S$), but the bound drug concentration remains non-zero: as diffusion proceeds, more bound drug is permitted to dissolve until eventually $b_0 = 0$. In this case the rate of release is controlled by the solubility and the diffusion and we may simply select a value of β_0 such that $Da_0^* \gg 1$.

3.2. Spatially independent model for dissolution

It is of interest to investigate the similarities and differences between the models (3.1)–(3.2) for the three values of α. In this subsection we focus on the dissolution kinetics alone and consider the corresponding spatially independent models by neglecting the diffusive component. We assume that initially we have $b_0(0) = B > S$ and $c_0(0) = 0$. In addition we assume conservation of mass, that is, $b_0(t) + c_0(t) = B$. We adopt an analytic approach to solving the model for each value of α. We scale all concentrations as in Eq. (3.3) and time as $t^* = \beta_0 B^{\alpha} t$.

$\alpha = 0$: In this case the model is linear and we obtain the solution for the concentrations of encapsulated and dissolved drug:

$$b_0' = 1 - S'[1-\exp(-t^*)], \quad c_0' = S'[1-\exp(-t^*)].$$

$\alpha = 1$: For this case the model is nonlinear but it is still straightforward to get an exact solution for the concentrations:

$$b_0' = \frac{S'-1}{S'\exp[(S'-1)t^*]-1}, \quad c_0' = \frac{S'\{\exp[(S'-1)t^*]-1\}}{S'\exp[(S'-1)t^*]-1}.$$

$\alpha = 2/3$: When $\alpha = 2/3$ we obtain an implicit expression for b_0':

$$\ln \frac{\left(b_0'^{1/3}+G\right)\left(1-G+G^2\right)^{1/2}}{(1+G)\left(b_0'^{2/3}-b_0'^{1/3}G+G^2\right)^{1/2}} + \sqrt{3}\left\{\arctan\left\{\frac{1}{\sqrt{3}}\left(\frac{2b_0'^{1/3}}{G}-1\right)\right\}-\arctan\left\{\frac{1}{\sqrt{3}}\left(\frac{2}{G}-1\right)\right\}\right\} = -G^2 t^* \tag{3.5}$$

with $G=(S'-1)^{1/3}$. We note that in this case the solution can be obtained numerically by using any standard nonlinear root-solver. We can then get $c_0' = 1-b_0'$.

From the analytic solutions for $\alpha = 0$ and $\alpha = 1$, it is evident that in equilibrium ($t\to\infty$), $c_0' = S'$ and $b_0' = 1-S'$. Although not immediately obvious from Eq. (3.5), the equilibrium values for the case of $\alpha = 2/3$ are identical to those obtained for other values of α and the differences occur in the transient only. In Fig. 3 we compare the three different models by plotting normalized dissolved and encapsulated drug concentration profiles against normalized time.

The three profiles are virtually indistinguishable for small S' (not displayed). However, as we increase S', the differences are magnified. We observe that the linear model ($\alpha = 0$) results in the quickest rate of dissolution, while the nonlinear models result in slower dissolution with increasing α, with $\alpha = 1$ having the slowest dissolution rate. As a consequence, the $\alpha = 0$ case reaches equilibrium first, followed by the $\alpha = 2/3$ and $\alpha = 1$ cases, respectively. It is also interesting to note that as we increase S', not only does the equilibrium value of the dissolved drug increase, but also the time taken to reach equilibrium increases. Although this analysis has neglected the spatial distribution of drug, it is anticipated that the above trends will hold when diffusion is included, albeit the dissolution will be quicker due to the continuous clearance of drug from the coating.

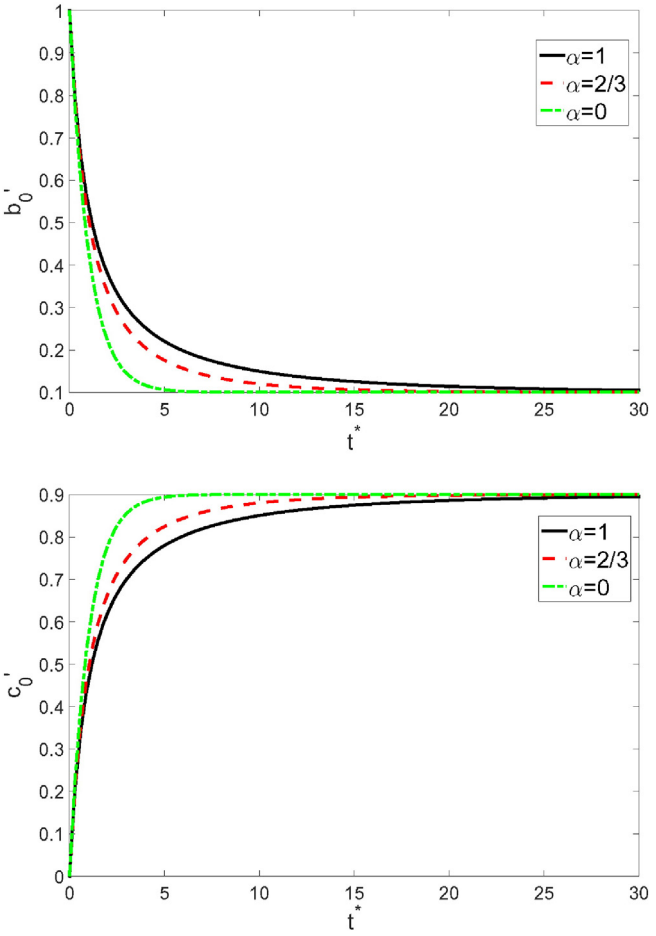

Fig. 3. Comparison of the time evolution of encapsulated (top) and dissolved (bottom) drug concentrations for $\alpha = 0$, $\alpha = 2/3$, $\alpha = 1$ and $S' = 0.9$. As S' is reduced (not shown), the equilibrium c_0' value is reduced and occurs sooner and the three curves become closer together until they eventually overlap.

4. Modelling drug dynamics and absorption in the biological tissue

Following the dissolution process, the now biologically available drug diffuses through the polymeric layer and, due to a concentration jump, a mass flux is established across the interface and the drug starts to be transferred to the adjacent release medium. For the purposes of this paper we make the assumption that the biological tissue comprises a single homogeneous layer exhibiting isotropic diffusion properties. However, depending on the DDD, it may be more appropriate to consider multiple tissue layers [13]. Within the tissue the free drug (c_1) undergoes diffusion, with a possible convective flux due to a pressure gradient across the tissue. Finally, to exert its therapeutic effect, a fraction of the free drug binds to binding sites (b_1).

4.1. Drug binding models

Depending on the drug and the device application, the binding model may be linear or nonlinear, saturable or non-saturable, reversible or irreversible. We start with the most general of these, the nonlinear saturable reversible binding model, having its roots in molecular cell biology [27]. The model describes the reversible binding of ligands (free drug molecules) with receptors (free binding sites) to form complexes:

$$\text{ligand} + \text{receptor} \underset{k_1^r}{\overset{k_1^f}{\rightleftharpoons}} \text{complex},$$

where, k_1^f is the association (forward) rate constant which characterizes the velocity of the second-order interaction between the receptor and ligand while k_1^r is the dissociation (backward) rate constant and characterizes the velocity of the first-order breakdown of the receptor/ligand complex. The two rate constants depend upon the porosity of the tissue and are related through the equilibrium dissociation constant, $K_d = k_1^r/k_1^f$ (or the equilibrium association constant, $K_a = 1/K_d$). It is reasonable to assume a conservation condition for binding sites, that is the number of occupied and free binding sites is equal to the local density of binding sites, b_{max}. Adopting this model, we can write an equation for the rate of change of bound drug, b_1 [28]:

$$\frac{db_1}{dt} = k_1^f c_1 (b_{max} - b_1) - k_1^r b_1. \tag{4.1}$$

The above equation is well accepted to describe binding-unbinding processes in biological media, and has been used by several other authors in various contexts, including for drug release to the arterial wall [28,15] and tumour drug delivery [28,29]. Loosely speaking, binding describes a phenomenon opposite to dissolution, and Eq. (4.1), with the unbinding rate set to zero, is formally similar, except for the sign, to the $\alpha = 1$ dissolution model in Eq. (3.1).

4.2. Special cases

In order to demonstrate the generality of the proposed binding model, we now show how three other binding models can be seen to be special cases of Eq. (4.1).

(a) Nonlinear saturable irreversible binding

This model is obtained from Eq. (4.1) by choosing $k_1^r = 0$ and may be appropriate in cases where drug binds with sites to form a complex that is retained on the time-scale of interest.

(b) Linear reversible binding

The linear binding model assumes first order linear reaction kinetics, where the rate of change of bound drug concentration is proportional (via β_1) to the distance from the equilibrium value (K_a times the free drug concentration):

$$\frac{db_1}{dt} = \beta_1\left(c_1 - \frac{b_1}{K_a}\right) = \beta_1 c_1 - \delta_1 b_1. \tag{4.2}$$

Initially, the rate of uptake to the bound phase is rapid since $b_1 = 0$ at $t = 0$, but this rate reduces with increasing b_1 until the equilibrium is reached, at which point the sign inside the brackets in Eq. (4.2) changes and drug is released back into the free phase. An important difference between this model and the general model (4.1) is that the former is non-saturable. This first order reaction model is appropriate when the drug uptake and release processes proceed at a rate that depends linearly on only one concentration (free and bound, respectively).

(c) Linear irreversible binding.

In this model the drug is irreversibly transferred from the free phase at a rate of β_1 and is lost from the system, i.e.:

$$\frac{db_1}{dt} = \beta_1 c_1. \tag{4.3}$$

This model, neither reversible nor saturable, may be appropriate in cases where drug is consumed ('*metabolized*') within the bound phase or removed from the system via, for example, blood vessels in the arterial wall.

It is easily shown that Eqs. (4.2) and (4.3) can be seen to be special cases of Eq. (4.1). Firstly, let us rescale b_1 as follows:

$$\bar{b}_1 = \frac{b_1}{c^*}, \qquad \bar{c}_1 = \frac{c_1}{c^*}$$

where c^* is taken to be a representative drug concentration in the tissue. Then Eq. (4.1) becomes

$$\frac{d\bar{b}_1}{dt} = k_1^f \bar{c}_1 b_{max}\left(1 - \frac{c^*}{b_{max}}\bar{b}_1\right) - k_1^r \bar{b}_1. \tag{4.4}$$

Immediately we see that if the density of binding sites is far greater than the drug concentration they are exposed to, i.e. if

$$\frac{c^*}{b_{max}} \ll 1, \tag{4.5}$$

then Eq. (4.4) reduces to

$$\frac{d\bar{b}_1}{dt} = k_1^f b_{max}\bar{c}_1 - k_1^r \bar{b}_1, \tag{4.6}$$

which is of the form Eq. (4.2). We note that condition (4.5) may be satisfied for the duration of release in cases where the binding site density is very large. However, even if the binding site density is relatively low compared with the applied drug concentration, this condition may well be satisfied at early times, when the tissue concentrations are still sufficiently low. If, in addition to Eq. (4.5), the reverse reaction rate is zero, then we return Eq. (4.3).

4.3. Drug tissue transport

Finally, the equations of drug transport in the tissue take account of possible convection (of magnitude v_1), diffusion (with diffusion coefficient D_1) and the binding reaction as described by Eq. (4.1):

$$\frac{\partial c_1}{\partial t} = D_1\frac{\partial^2 c_1}{\partial x^2} - v_1\frac{\partial c_1}{\partial x} - k_1^f c_1(b_{max} - b_1) + k_1^r b_1 \qquad \text{in}(0, l_1) \tag{4.7}$$

$$\frac{\partial b_1}{\partial t} = k_1^f c_1(b_{max} - b_1) - k_1^r b_1 \qquad \text{in}(0, l_1). \tag{4.8}$$

In principle, the specific drug under consideration may bind to more than one component of the biological tissue (see e.g. [5]), resulting in additional bound phases of drug. The result would be additional reaction terms in Eq. (4.7) as well as an additional binding reaction equation of the form Eq. (4.8) for each bound phase. For details of how this may be incorporated within the general model, we refer the reader to the Appendix 0. It is recognized that for some applications, drug binding may be rapid. In this case, if the resulting Damköhler number is so large that binding is diffusion limited, the concentrations of free and bound drug may exist in quasi-equilibrium and the model may be simplified. For further details the reader is referred to [21,28]. It is noted, however, that the low computational cost of the numerical method described in this paper means that the solving of the full model (even if binding is fast) does not significantly add to the computation time.

5. A coupled two-layer system

We now couple the general model for drug dissolution–diffusion in the coating Eqs. (3.1)–(3.2), with the model of convection-diffusion and nonlinear binding in the wall Eqs. (4.7)–(4.8) by introducing appropriate boundary, initial and interface conditions.

5.1. Boundary, interface and initial conditions

To close the two-layer two-phase mass transfer system Eqs. (3.1)–(3.2) and Eqs. (4.7)–(4.8), a flux continuity condition has to be assigned at the interface between the polymer coating and the tissue:

$$-D_0\frac{\partial c_0}{\partial x} = -D_1\frac{\partial c_1}{\partial x} + vc_1 \quad \text{at} \quad x = 0.$$

Additionally, a concentration jump may occur:

$$-D_1\frac{\partial c_1}{\partial x} = P(c_0 - c_1) \quad \text{at} \quad x = 0,$$

with $P(cm/s)$ the overall mass transfer coefficient. The case of no concentration jump is obtained as a limiting case with $P \to \infty$. In keeping with the generality of the model, we assume a Robin-type boundary condition at both $x = -l_0$ and $x = l_1$. We therefore have

$$-D_0\frac{\partial c_0}{\partial x} = \gamma_0 c_0 \qquad \text{at} \quad x = -l_0,$$

and

$$-D_1\frac{\partial c_1}{\partial x} + v_1 c_1 = \gamma_1 c_1 \quad \text{at} \quad x = l_1.$$

The constants γ_0 and γ_1 can be adjusted so that the fluxes match experimentally observed conditions. For example, in the case of drug-eluting stents, if significant amounts of drug are lost to the flowing blood, then the parameter γ_0 can be adjusted to account for this. We note that zero flux and infinite sink conditions can be recovered by letting γ_0, γ_1 tend to zero and infinity, respectively. The initial

conditions are:

$$b_0(x,0)=B,\quad c_0(x,0)=0,\quad c_1(x,0)=0,\quad b_1(x,0)=0\,.$$

5.2. Nondimensionalization

We introduce the typical nondimensionalization for a system of reaction–diffusion-convection equations, leading to two relevant numbers: the Péclet (*Pe*) and the Damköhler number (*Da*). These dimensionless groups define, respectively, the relative importance of convection to diffusion, and of reaction to diffusion. By examining their size, it is often possible to simplify the model by neglecting parameters that are unimportant. For the coupled system we nondimensionalize space and time with the parameters of layer 1:

$$x'=\frac{x}{l_1},\quad t'=\frac{D_1 t}{l_1^2}.$$

and, following nondimensionalization in Eq. (3.3), we scale all the remaining concentrations with B:

$$b_1'=\frac{b_1}{B},\quad c_1'=\frac{c_1}{B},\quad b'_{max}=\frac{b_{max}}{B}.$$

Let us now define the following dimensionless parameters:

$$\begin{aligned} &D=\frac{D_0}{D_1},\quad L=\frac{l_0}{l_1},\quad Da_0^{(\alpha)}=\frac{\beta_0 B^{\alpha-1}Sl_1^2}{D_1},\quad \Gamma_0=\frac{\gamma_0 l_1}{D_1}\quad \Pi=\frac{Pl_1}{D_1}\\ &Pe=\frac{v_1 l_1}{D_1},\quad Da_1=\frac{k_1^f l_1^2 b_{max}}{D_1},\quad B_p=\frac{b_{max}}{K_d},\quad \Gamma_1=\frac{\gamma_1 l_1}{D_1}. \end{aligned} \tag{5.1}$$

B_p is referred to as the binding potential and measures the affinity of a drug to a given receptor.

Summarizing, the governing equations (after dropping primes for clarity) are the following:

$$\frac{\partial b_0}{\partial t}=-Da_0^{(\alpha)}b_0^{\alpha}\left(1-\frac{c_0}{S}\right) \quad \text{in}\quad (-L,0), \tag{5.2}$$

$$\frac{\partial c_0}{\partial t}=D\frac{\partial^2 c_0}{\partial x^2}+Da_0^{(\alpha)}b_0^{\alpha}\left(1-\frac{c_0}{S}\right) \quad \text{in}\quad (-L,0), \tag{5.3}$$

$$\frac{\partial c_1}{\partial t}=\frac{\partial^2 c_1}{\partial x^2}-Pe\frac{\partial c_1}{\partial x}-Da_1\left(c_1\left(1-\frac{b_1}{b_{max}}\right)-\frac{b_1}{B_p}\right) \quad \text{in}\quad (0,1), \tag{5.4}$$

$$\frac{\partial b_1}{\partial t}=Da_1\left(c_1\left(1-\frac{b_1}{b_{max}}\right)-\frac{b_1}{B_p}\right) \quad \text{in}\quad (0,1), \tag{5.5}$$

$$-\frac{\partial c_0}{\partial x}=\Gamma_0 c_0 \quad \text{at}\quad x=-L, \tag{5.6}$$

$$-\frac{D\partial c_0}{\partial x}=-\frac{\partial c_1}{\partial x}+Pe\,c_1 \quad \text{at}\quad x=0, \tag{5.7}$$

$$-\frac{D\partial c_0}{\partial x}=\Pi(c_0-c_1) \quad \text{at}\quad x=0, \tag{5.8}$$

$$-\frac{\partial c_1}{\partial x}+Pec_1=\Gamma_1 c_1 \quad \text{at}\quad x=1. \tag{5.9}$$

6. Numerical solution

We proceed to solve the nondimensional system Eqs. (5.2)–(5.9) numerically. Let us subdivide the interval $(-L,0)$ into $N+1$ equispaced grid nodes $x_j=(j-N)\,h_0,\quad j=0,1,..,N$, and the interval (0,1) with $M+1$ equispaced points $x_j=j\,h_1,\quad j=0,1,...,M$. Here, h_0 and h_1 represent the spacing in the coating and tissue layers, respectively. Let us indicate by a superscript j the approximated value of the concentrations at x_j.

In each layer, we approximate the diffusive terms by considering a standard finite difference of the second derivative at internal nodes x_j:

$$\left.\frac{\partial^2 c_0}{\partial x^2}\right|_{x_j}\simeq\frac{c_0^{j-1}-2c_0^j+c_0^{j+1}}{h_0^2}\quad j=1,...,N-1\,, \tag{6.1}$$

$$\left.\frac{\partial^2 c_1}{\partial x^2}\right|_{x_j}\simeq\frac{c_1^{j-1}-2c_1^j+c_1^{j+1}}{h_1^2}\quad j=1,...,M-1\,. \tag{6.2}$$

The reaction terms in Eqs. (5.3)–(5.4) do not contain any derivatives and therefore are discretized pointwise. For example, Eq. (5.3) is discretized at node x_j as:

$$\left.\frac{dc_0^j}{dt}\right|_{x_j}=D\frac{c_0^{j-1}-2c_0^j+c_0^{j+1}}{h_0^2}+Da_0^{(\alpha)}\left(b_0^j\right)^{\alpha}\left(1-\frac{c_0^j}{S}\right). \tag{6.3}$$

At the boundary points $x=-L$ and $x=1$ we assume Eqs. (5.2)–(5.5) hold, but the approximations (6.1)–(6.2) are modified taking into account the boundary conditions (5.6) and (5.9).

6.1. Treatment of the interface

At the interface $x=0$, we potentially have a discontinuity in concentration and two possibly different values, say $\tilde{c}_0^N$ and $\tilde{c}_1^0$ (the tilde accent indicates these special points), one for each interface side, need to be determined (Fig. 4).

No derivative can be computed across the interface $x=0$, due to a possible discontinuity and approximations Eqs. (6.1)–(6.2) no longer apply. An alternative procedure is needed to get $\tilde{c}_0^N$ for Eq. (6.1) for $j=N-1$ and $\tilde{c}_1^0$ for Eq. (6.2) for $j=1$. Their values are related through the interface conditions (5.7)–(5.8):

$$\begin{aligned} -D\frac{\partial c_0^N}{\partial x}&=-\frac{\partial c_1^0}{\partial x}+Pe\tilde{c}_1^0\\ -D\frac{\partial c_0^N}{\partial x}&=\Pi\left(\tilde{c}_0^N-\tilde{c}_1^0\right) \end{aligned}. \tag{6.4}$$

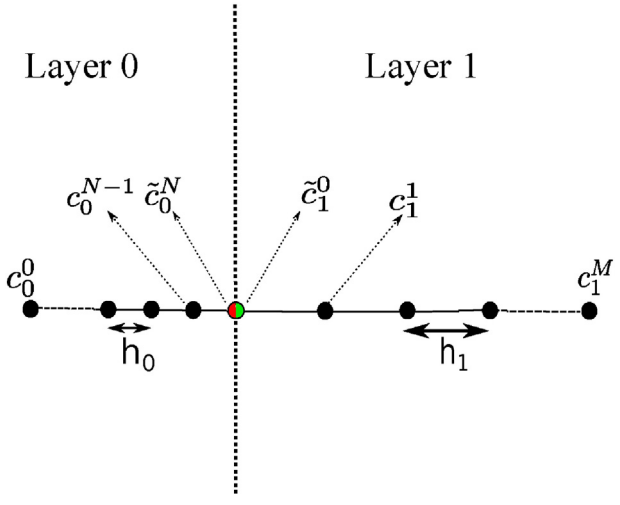

Fig. 4. Illustration of grid nodes in the two layers and the interface points (in red and green). They are computed a posteriori as a linear combination of the neighbouring grid points (Eqs. (6.6)–(6.7)). (For interpretation of the references to colour in this figure legend, the reader is referred to the web version of this article.)

Following the technique described by Hickson et al. [30], we take a Taylor series expansion for $c_0^{N-2}, c_0^{N-1}, c_1^1, c_1^2$, and arrive at:

$$\begin{aligned} c_0^{N-1} &\approx \tilde{c}_0^N - h_0 \frac{\partial \tilde{c}_0^N}{\partial x} + \frac{h_0^2}{2}\frac{\partial^2 \tilde{c}_0^N}{\partial x^2}. \\ c_0^{N-2} &\approx \tilde{c}_0^N - 2h_0 \frac{\partial \tilde{c}_0^N}{\partial x} + 2h_0^2 \frac{\partial^2 \tilde{c}_0^N}{\partial x^2} \\ c_1^1 &\approx \tilde{c}_1^0 + h_1 \frac{\partial \tilde{c}_1^0}{\partial x} + \frac{h_1^2}{2}\frac{\partial^2 \tilde{c}_1^0}{\partial x^2} \\ c_1^2 &\approx \tilde{c}_1^0 + 2h_1 \frac{\partial \tilde{c}_1^0}{\partial x} + 2h_1^2 \frac{\partial^2 \tilde{c}_1^0}{\partial x^2} \end{aligned} \tag{6.5}$$

The two equations in Eq. (6.4) and the four equations in Eq. (6.5) form an algebraic system of six equations that allows one to express $\tilde{c}_0^N, \tilde{c}_1^0$ and their first and second derivatives as a linear combination of the neighbouring values. It can be shown that

$$\tilde{c}_0^N = \frac{D[3 + 2h_1(\Pi + Pe)](4c_0^{N-1} - c_0^{N-2}) + 2h_0\Pi(4c_1^1 - c_1^2)}{R} \tag{6.6}$$

$$\tilde{c}_1^0 = \frac{(3D + 2h_0\Pi)(4c_1^1 - c_1^2) + 2Dh_1\Pi(4c_0^{N-1} - c_0^{N-2})}{R} \tag{6.7}$$

where $R = 9D + 6\Pi(Dh_1 + h_0) + 2h_1 Pe(3D + 2h_0\Pi)$.

After spatial discretization, the system of PDEs reduces to a system of nonlinear ordinary differential equations (ODEs) of the form:

$$\frac{dY}{dt} = A(Y), \tag{6.8}$$

where $Y = (b_0^0, ..., b_0^{N-1}, c_0^0, ..., c_0^{N-1}, c_1^1, ..., c_1^M, b_1^1, ..., b_1^M)^T$ and $A(Y)$ contains the $2(N + M)$ discretized Eqs. (5.2)–(5.9). The system (6.8) is solved by the routine ode15s of Matlab based on a Runge–Kutta type method with backward differentiation formulas, and an adaptive time step [31]. The interface free drug concentrations $\tilde{c}_0^N, \tilde{c}_1^0$ are computed a posteriori through Eqs. (6.6)–(6.7) and the corresponding bound concentrations $\tilde{b}_0^N, \tilde{b}_1^0$ are obtained by solving the first order ODEs (5.2) and (5.5) analytically. In principle, negative values of b_0 may occur, since Eq. (5.2) holds only for the period during which dissolution is ongoing. We handle this numerically by setting the source term in Eqs. (5.2)–(5.3) to zero when $b_0 < 0$.

In order to verify the correctness of the numerical code, it is useful to compare the numerical solution to any available analytical solutions. Unfortunately, analytical solutions for the full model are not available due to the complexity of the two-layer four-phase nonlinear model. However, we have performed a number of checks which give confidence in our numerical results. Firstly, we have checked the results of the code against an analytically solvable diffusion model in composite media [32]. Secondly, we have imposed zero flux conditions at $x = -L$ and $x = 1$ and evaluated the total mass of drug in the system with time to ensure mass conservation.

7. A case study: The drug-eluting stent

To demonstrate the utility of the model we focus on the particular application of drug-eluting stents (Fig. 1). Stents are tubular wire mesh devices inserted into coronary arteries which have narrowed as a result of a pathological condition called atherosclerosis. Besides the mechanical support due to the scaffold-like array of struts, the purpose of the drug-eluting stent is to deliver a local dose of anti-proliferative/anti-inflammatory medication to counter the effects of restenosis [1]. For this application, diffusion, binding and convection all occur in the arterial tissue, with the latter appearing as a result of the transmural pressure gradient across the wall.

One of the great difficulties in the modelling of biological systems is obtaining accurate estimates of the various parameters. In the case of drug eluting stents, there exists a plethora of data in the literature. However, the degree of variability of the estimates of some of the parameters is substantial. It is usual for them to be estimated based on experiments with a small number of repetitions, and in some cases lumped diffusion coefficients (which inherently include such effects as transmural convection and binding) are calculated. Furthermore, the transport properties vary from species to species and may well vary substantially between tissue samples of the same species. Therefore, for the purposes of this paper, we have decided to provide an indicative range for the parameters where a unique value has not been reported. These are displayed in Table 1 along with the actual values used in the simulations. A full sensitivity study for a particular DDD is beyond the scope of this work, which focuses on the presentation of a general model. However, we have decided to select parameter values from the stated ranges based on two criteria. Firstly, we wish to demonstrate that the model can predict the correct duration of in-vivo release and secondly, we seek qualitative agreement with experimentally observed mass of drug in the tissue as a function of time.

The stent coating parameters are representative of a first generation polymer coated drug-eluting stent (Cypher Stent), whilst the binding parameters have been taken from Tzafriri et al. [28] (Table 1). We note that in the absence of data on the parameter β_0, we have chosen a value such that diffusion is the slowest process. For the simulated parameter values, we are in the regime of case 2) of Section 3.1. In addition we choose the values of γ_0 and γ_1 such that we have a zero flux condition at the impermeable stent strut ($x = -l_0$), and zero drug concentration at the extent of the tissue ($x = l_1$).

Using the parameter values of Table 1, we simulate the concentration profiles for free and bound drug in both the coating and the tissue, b_0, c_0, c_1, b_1. As described in Section 6, we solve the model numerically

Table 1
Dimensional parameter values used in the simulations for the case of the drug-eluting stent. The values chosen are representative of the extensive literature.

Parameter	Indicative range	Simulated value	References
γ_0	0 cm s^{-1}	0 cm s^{-1}	[16,17]
α	0 − 1	2/3	[8,26,14]
D_0	$\mathcal{O}(10^{-12})$ cm^2 s^{-1}	$1.2\cdot10^{-12}$ cm^2 s^{-1}	[16]
l_0	$\mathcal{O}(10^{-3})$ cm	10^{-3} cm	[16]
β_0	$>> D_0/(B^\alpha l_0^2)$ s^{-1} $(mol\ cm^{-3})^{-2/3}$	1 s^{-1} $(mol\ cm^{-3})^{-2/3}$	–
B	10^{-4} mol cm^{-3}	10^{-4} mol cm^{-3}	[15]
S	$B/10$	$B/10$	[21]
P	10^{-6} cm s^{-1}	10^{-6} cm s^{-1}	[17]
v	$10^{-6} - 10^{-5}$ cm s^{-1}	$5.8\cdot10^{-6}$ cm s^{-1}	[5,16,17]
D_1	$\mathcal{O}(10^{-9})-\mathcal{O}(10^{-6})$ cm^2 s^{-1}	$2.5\cdot10^{-6}$ cm^2 s^{-1}	[5,15]
l_1	$4.5\cdot10^{-2}$ cm	$4.5\cdot10^{-2}$ cm	[33]
k_1^f	$2\cdot10^6$ $(mol\ cm^{-3}\ s)^{-1}$	$2\cdot10^6$ $(mol\ cm^{-3}\ s)^{-1}$	[28]
k_1^r	$5.2\cdot10^{-3}$ s^{-1}	$5.2\cdot10^{-3}$ s^{-1}	[28]
b_{max}	$3.66\cdot10^{-7}$ mol cm^{-3}	$3.66\cdot10^{-7}$ mol cm^{-3}	[28]
$1/\gamma_1$	0 cm s^{-1}	0 cm s^{-1}	[5,15,16]

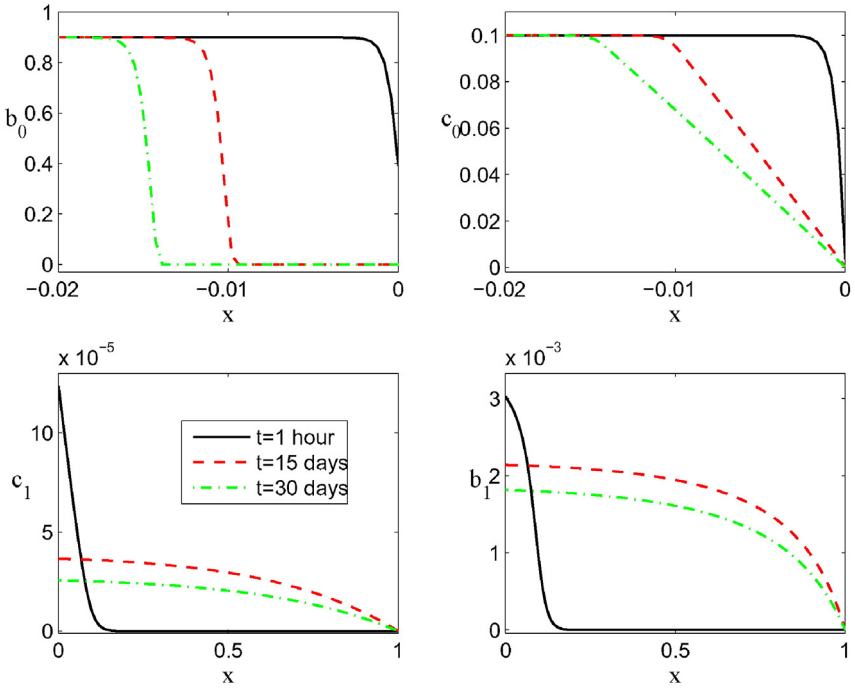

Fig. 5. Nondimensional concentration profiles at three times. In each layer, both bound and free concentrations are depicted.

by first spatially discretizing the equations and then employing the routine ode15s of Matlab which includes an adaptive time step. In order to provide confidence in the numerical simulations we conducted a grid refinement study. Briefly, we increased the number of grid nodes until the resulting concentration values varied by less than 1%. As a result, the final numerical code included 50 coating grid nodes and 200 tissue grid nodes.

In Fig. 5, concentration profiles at 1 hour, 15 and 30 days are displayed. Note the sharp boundary layer at early times. The free drug phase in the coating is saturated rapidly ($c_0 = S = 0.1$), but b_0 remains non-zero: as diffusion proceeds, more bound drug is permitted to dissolve. Even after 30 days, bound drug exists within the coating, albeit situated near to the boundary between the coating and the strut. Drug diffuses through the free phase in the coating and enters the biological

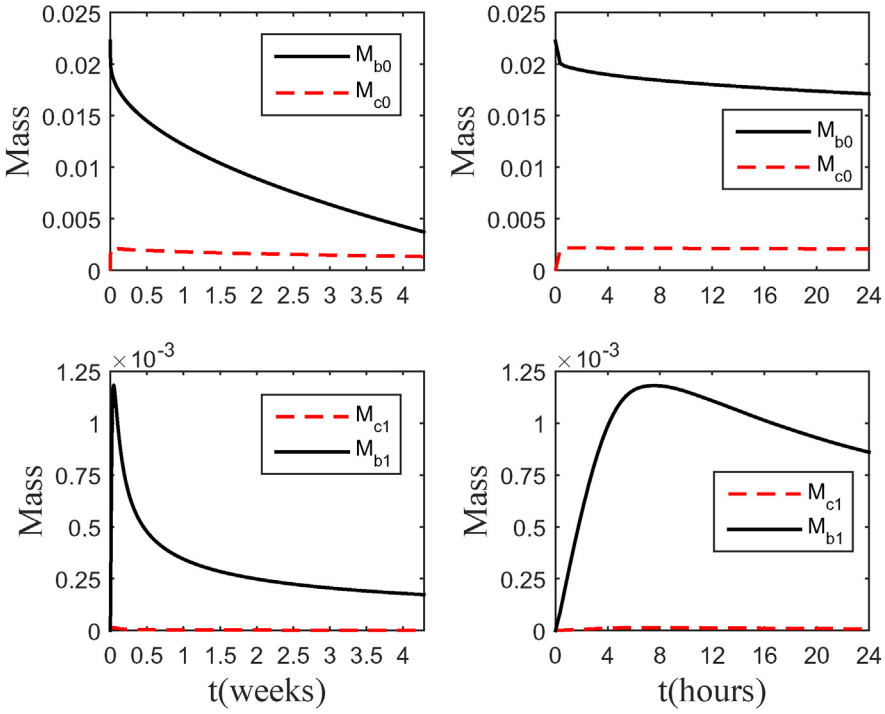

Fig. 6. Nondimensional drug mass in the coating (top) and wall (bottom) as a function of time. The plots on the right are magnifications of the plots on the left over the first 24 hours. Only the coating encapsulated drug mass is monotonically decreasing while all the other phases have a characteristic time at which the drug mass reaches a peak. Note the sharp gradient of M_{b0} and M_{c0} close to the initial time.

Table 2
Percentage of drug mass retained in each phase at different times for the simulated parameters in Table 1. With the exception of the coating encapsulated phase, the mass of drug in all the other phases starts from zero and reaches a peak before decaying with time. The negligible values of θ_{c1} only serve to highlight that drug preferentially accumulates within the bound phase in the tissue. The percentage of drug released by 30 days is calculated as $100-\theta_{b0}-\theta_{c0}$ and is compared with in-vivo experimental data.

t (days)	θ_{b0}	θ_{c0}	θ_{c1}	θ_{b1}
0.02	90.4	9.1	0.0	0.4
0.05	88.6	9.7	0.0	1.4
0.08	87.6	9.7	0.0	2.3
0.13	86.1	9.7	0.0	3.8
1.5	74.0	9.1	0.0	3.2
7.5	53.5	8.0	0.0	1.5
15.0	38.2	7.1	0.0	1.1
22.5	26.5	6.5	0.0	0.9
30.0	16.7	6.0	0.0	0.8
		Model	Experimental data [5]	
% released by 30 days		77.3	82.5	

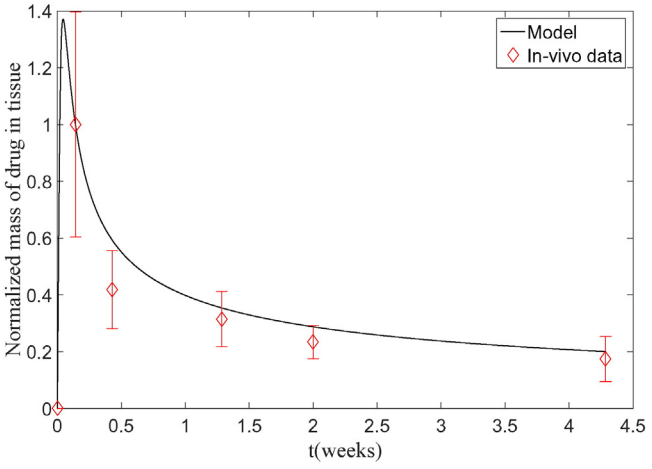

Fig. 7. Comparison between model and experimental results [5] for total mass of drug in tissue. Values have been normalized with respect to the mass at the first experimental time point (day 1).

tissue, where the free and bound tissue drug concentrations rise to a peak (not shown) before reducing with time as drug traverses through the tissue and is absorbed at the far boundary. The values of b_1 are typically two orders of magnitude higher than c_1, owing to the strong binding potential. The result is that most of the drug in the tissue is contained within the bound phase (Fig. 6).

The drug mass in each phase is easily computed as an integral of the concentration over the corresponding layer:

$$M_j(t) = \int j(x,t)dx, \quad j = b_0, c_0, c_1, b_1. \tag{7.1}$$

Furthermore, the fraction of drug mass retained in each layer and phase is computed as

$$\theta_j(t) = \frac{M_j(t)}{M_{b0}(0)}, \quad j = b_0, c_0, c_1, b_1. \tag{7.2}$$

These are useful indicators of drug release, diffusion and absorption. In Fig. 6 we plot the nondimensional mass in each phase as a function of time, whilst in Table 2 we present the percentage of drug retained in each phase for different times up to 30 days.

As a consequence of the rapid dissolution rate, we observe a sharp gradient close to the initial time, where the free drug mass increases very quickly from zero to saturation levels (Fig. 6, top). For the remainder of the 30 days simulated, the free drug stays at this saturated level, indicating that the rate of release is being controlled by both the drug solubility and the rate of diffusion in the polymer coating. Fig. 6 (bottom) shows that both the free and the bound drug masses rise from zero to a peak within 1 day. The peak mass of bound drug, substantially higher than that of free drug, occurs when all of the binding sites become saturated: after this time, we observe a slow decay of b_1 as drug unbinds into the free phase and diffuses out of the tissue.

We point out that for the simulated parameter values, the model reproduces a biphasic release profile with an initial burst followed by an approximately linear profile for the duration of the 30 days (Fig. 6 (top)). The simulated duration of release (77.3% by 30 days, Table 2) compares well with existing in-vivo experimental data (82.5% by 30 days) [5]. Additionally, when we compare the simulated results of the variation in total mass of drug in the tissue with the corresponding in-vivo experimental data (Fig. 7) we find good agreement.

8. Conclusions

Besides being a relevant bioengineering application, modelling drug delivery from a DDD constitutes a challenging problem from a mathematical and computational point of view. Any proposed model should be founded on a balance between generality (flexible and able to describe a number of different cases), reliability (able to capture the qualitative behaviour) and simplicity (only include the important features and be easy to use). The reality is that biological systems are extremely complex and some degree of simplification is necessary if any progress is to be made. We believe that the proposed model represents a sufficiently good compromise between these modelling requirements.

In this paper we have presented a general and unified model of drug release and tissue distribution that may be applied to a number of drug delivery systems. Our model accounts for the combined effects of diffusion, dissolution and solubility in the polymer coating and can model several different types of binding in the tissue, ranging from nonlinear saturable reversible to linear irreversible binding. By presenting the case of a drug-eluting stent, we have been able to demonstrate that the model can provide results which are consistent with in-vivo experimental data, and moreover, provides added value over experiments in that concentration profiles can be calculated for the drug in each phase - this is virtually impossible to do by experiments alone. The proposed model will be useful to better understand the drug release kinetics of existing DDD, and in designing those of the future.

Acknowledgements

Dr. McGinty would like to acknowledge the funding provided by EPSRC under grant number EP/J007242/1.

Appendix 0

In this appendix we outline how multiple bound phases in the tissue may be incorporated within the general model. The concentration of drug that is bound to component i is given by b_1^i whilst the density of binding sites associated with that component is given by $b^i_{\max}$ and the respective forward and backward rate constants are given by $k_1^{i,f}$ and $k_1^{i,r}$. With n the total number of different components for which drug can bind to, Eqs. (4.7)–(4.8) are then replaced by

$$\frac{\partial c_1}{\partial t} = D_1\frac{\partial^2 c_1}{\partial x^2} - v_1\frac{\partial c_1}{\partial x} - \sum_{i=1}^{n}\left\{k_1^{i,f}c_1\left(b^i_{max}-b_1^i\right) - k_1^{i,r}b_1^i\right\} \quad \text{in } (0,l_1) \tag{8.3}$$

$$\frac{\partial b_1^i}{\partial t} = k_1^{i,f}c_1\left(b^i_{max}-b_1^i\right) - k_1^{i,r}b_1^i, \quad i = 1,\ldots,n \quad \text{in} \quad (0,l_1). \tag{8.4}$$

References

[1] S. McGinty, A decade of modelling drug release from arterial stents, Math. Biosci. 257 (2014) 80–90.
[2] W.E. Zhang, M.R. Prausnitz, A.U. Edwards, Model of transient drug diffusion across cornea, J. Control. Release 99 (2004) 241–258.
[3] M.R. Prausnitz, R. Langer, Transdermal drug delivery, Nat. Biotechnol. 26 (11) (2008) 1261–1268.
[4] J.A. Lyndon, B.J. Boyd, N. Birbilis, Metallic implant drug/device combinations for controlled drug release in orthopaedic applications, J. Control. Release 179 (2014) 63–75.
[5] A.R. Tzafriri, A. Groothuis, G. Sylvester Price, E.R. Edelman, Stent elution rate determines drug deposition and receptor-mediated effects, J. Control. Release 161 (2012) 918–926.
[6] F. Bozsak, D. Gonzalez-Rodriguez, Z. Sternberger, P. Belitz, T. Bewley, J.M. Chomaz, A.I. Barakat, Optimization of drug delivery by drug-eluting stents, PLoS One 10 (6) (2015), e0130182.
[7] R. Langer, Polymeric delivery systems for controlled drug release, Chem. Eng. Commun. 6 (1980) 1–48.
[8] G. Frenning, Modelling drug release from inert matrix systems: from moving-boundary to continuous-field descriptions, Int. J. Pharm. 418 (1) (2011) 88–99.
[9] J. Siepmann, F. Siepmann, Modelling of diffusion controlled drug delivery, J. Control. Release 161 (2012) 351–362.
[10] J. Siepmann, F. Siepmann, Mathematical modelling of drug dissolution, Int. J. Pharm. 453 (2013) 12–24.
[11] J. Siepmann, F. Siepmann, Mathematical modelling of drug delivery, Int. J. Pharm. 364 (2008) 328–343.
[12] S. Fredenberg, M.W.M. Reslow, A. Axelsson, The mechanisms of drug release in poly(lactic-co-glycolic acid)-based drug delivery systems — a review, Int. J. Pharm. 415 (2011) 34–52.
[13] G. Pontrelli, F. de Monte, A multi-layer porous wall model for coronary drug-eluting stents, Int. J. Heat Mass Transf. 53 (2010) 3629–3637.
[14] L. Formaggia, S. Minisini, P. Zunino, Modeling polymeric controlled drug release and transport phenomena in the arterial tissue, Math. Models Methods Appl. Sci. 20 (10) (2010) 1759–1786.
[15] F. Bozsak, J.M. Chomaz, A.I. Barakat, Modeling transport of drugs eluted from stents: physical phenomena driving drug distribution in the arterial wall, Biomech. Model. Mechanobiol. 13 (2) (2014) 327–347.
[16] S. McGinty, S. McKee, R.M. Wadsworth, C. McCormick, Modeling arterial wall drug concentrations following the insertion of a drug-eluting stent, SIAM J. Appl. Math. 73 (2013) 2004–2028.
[17] G. Pontrelli, F. de Monte, Mass diffusion through two-layer porous media: an application to the drug-eluting stent, Int. J. Heat Mass Transf. 50 (2007) 3658–3669.
[18] J.A. Ferreira, P. de Oliveira, P. Silva, J. Murta, Drug delivery: from a contact lens to the anterior chamber, *Comput. Model. Eng. Sci.* 71 (2011).
[19] L. Simon, N. Loney, An analytical solution for percutaneous drug absorption: application and removal of the vehicle, Math. Biosci. 197 (2005) 119–139.
[20] S. McGinty, G. Pontrelli, On the influence of solid–liquid mass transfer in the modelling of drug release from stents, J. Coupled Syst. Mult. Dyn. 3 (1) (2015) 47–56.
[21] S. McGinty, T. Vo, M. Meere, S. McKee, C. McCormick, Some design considerations for polymer-free drug-eluting stents: a mathematical approach, Acta Biomater. 18 (2015) 213–225.
[22] T. Higuchi, Rate of release of medicaments from ointment bases containing drugs in suspension, J. Pharm. Sci. 50 (1961) 874–875.
[23] D.R. Paul, S.K. McSpadden, Diffusional release of a solute from a polymer matrix, J. Membr. Sci. 1 (1976) 33–48.
[24] A. Noyes, W. Whitney, The rate of solution of solid substances in their own solutions, J. Am. Chem. Soc. 19 (1897) 930–934.
[25] A.W. Hixson, J.H. Crowell, Dependence of reaction velocity upon surface and agitation, Ind. Eng. Chem. 23 (1931) 923–931.
[26] G. Frenning, Theoretical investigation of drug release from planar matrix systems: effects of a finite dissolution rate, J. Control. Release 92 (2003) 331–339.
[27] D.A. Lauffenburger, J.J. Linderman, *Receptors: Models for Binding, Trafficking, and Signalling*, Oxford Univ. Press, New York, 1993.
[28] A.R. Tzafriri, A.D. Levin, E.R. Edelman, Diffusion-limited binding explains binary dose response for local arterial and tumour drug delivery, Cell Prolif. 42 (3) (2009) 348–363.
[29] C.M. Groh, M.E. Hubbard, P.F. Jones, et al., Mathematical and computational models of drug transport in tumours, J. R. Soc. Interface (2014) (online).
[30] R.I. Hickson, S.I. Barry, G.N. Mercer, H.S. Sidhu, Finite difference schemes for multilayer diffusion, Math. Comput. Model. 54 (2011) 210–220.
[31] L.F. Shampine, M.W. Reichelt, The MATLAB ODE suite, SIAM J. Sci. Comput. 18 (1997) 1–22.
[32] S. McGinty, S. McKee, R.M. Wadsworth, C. McCormick, Modelling drug-eluting stents, Math. Med. Biol. 29 (1) (2011) 1–29.
[33] X. Lu, J. Yang, J.B. Zhao, H. Gregersen, G.S. Kassab, Shear modulus of porcine coronary artery: contributions of media and adventitia, Am. J. Physiol. Heart Circ. Physiol. 285 (2003) H1966–H1975.